Prediction of Sound Fields in Cavities Using Boundary-Element Methods

R. J. Bernhard,* B. K. Gardner,† and C. G. Mollo†
Purdue University, West Lafayette, Indiana
and
C. R. Kipp‡
AT&T Bell Laboratories, Whippany, New Jersey

Two boundary-element formulations of acoustical behavior exist: the direct boundary-element methods based on the Helmholtz integral equations and the indirect boundary-element methods based on Huygen's principle. In this investigation, both methods are implemented utilizing a simple linear superparametric element. In addition, the indirect boundary-element method is studied using a quadratic isoparametric element. The accuracy and relative efficiency of the various techniques are examined. In order to model aircraft interior cavities properly, the additional capability to model wall treatments and internal point sources is added to the methods. The procedures are verified for several well-understood cavity problems. The relative merits of each boundary-element method is examined.

Introduction

LOW-FREQUENCY aircraft interior sound fields are a complicated function of geometry, source distribution, and cabin noise treatment. Numerical prediction procedures using generalized discretization techniques such as the finite- or boundary-element method have the powerful and flexible capabilities necessary to model interior cavities of aircraft. The finite-element method has been most widely used for such problems.[1,2] In this paper, the feasibility of boundary-element procedures for interior sound field prediction will be examined.

Boundary-element methods are numerical approximations to boundary integral equations. The most frequent use of boundary-element methods for acoustics in the past has been for infinite-domain problems such as studies of acoustic radiation or acoustic scattering.[3-10] Tanake et al.[11] have used the method for two-dimensional interior acoustical problems. In this investigation, the utility of the methods for three-dimensional interior problems is examined. In order to address the general interior noise problem, the capability to model wall treatments and acoustical point sources is also added to the previous formulations.

There are two boundary-element formulations of the acoustic problem.[12] Both are applicable to the interior noise problem and each will be examined. For the direct boundary-element method (DBEM), the primary variables of the problem—in this case acoustic pressure and velocity—are solved directly. The DBEM method utilizes the Helmholtz integral equations. For the indirect boundary-element method (IBEM), a secondary variable (a fictitious distribution of acoustic sources at the boundary) is solved. The primary variables at any point of interest are computed as a post-processing operation. The IBEM in acoustics is a numerical implementation of Huygen's principle.

Kipp[13] and Kipp and Bernhard[14] applied the indirect boundary-element method to the solution of interior acoustic fields using a quadratic isoparametric compatible boundary element. The results for spherical geometries having uniform velocity profiles were very good. The capability of applying point sources and impedance boundary conditions was also demonstrated. However, in rectangular cavities and situations with locally incompatible boundary conditions, the results were less encouraging. Kipp's studies suggest that incompatible elements are preferable to compatible elements for IBEM formulations. Furthermore, while the quadratic, isoparametric element is very accurate for the spherical geometries tested, the numerical implementation of such an element is significantly more complex than the more popular incompatible, linear superparametric elements often used for boundary-element programs. Thus, in the current investigations, Kipp's results are compared to results using linear superparametric elements for interior acoustical sound fields.

Direct Boundary-Element Formulation

The direct boundary-element formulations in acoustics utilize the Helmholtz integral equations, which can be written as

$$cp(\bar{x}_0) = \int_B [p(\bar{b})q^*(\bar{x}_0,\bar{b}) - q(\bar{b})p^*(\bar{x}_0,\bar{b})]\,dB \tag{1}$$

where p is the pressure distribution,

$$q = \frac{\partial p}{\partial n} = -i\omega\rho u \tag{2}$$

where $i = \sqrt{-1}$ and u is the normal velocity at the boundary,

$$p^* = e^{-ikr}/4\pi r \tag{3}$$

where

$$r = |\bar{x}_0 - \bar{b}| \tag{4}$$

and

$$q^* = \frac{\partial p^*}{\partial n} = \bar{n}\cdot\nabla p^* \tag{5}$$

Received May 19, 1986; presented as Paper 86-1864 at the AIAA 10th Aeroacoustics Conference, Seattle, WA, July 9-11, 1986; revision received Dec. 4, 1986. Copyright © American Institute of Aeronautics and Astronautics, Inc., 1987. All rights reserved.

*Assistant Professor, School of Mechanical Engineering, Ray W. Herrick Laboratories. Member AIAA.
†Research Assistant, School of Mechanical Engineering, Ray W. Herrick Laboratories.
‡Member of Technical Staff.

The coordinates $\bar{x}_0$ and $\bar{b}$ are defined in Fig. 1. The parameter c is defined as

$$\begin{aligned} c &= 0 \quad \text{for } X_0 \text{ outside } D \\ &= \tfrac{1}{2} \quad \text{for } X_0 \text{ at a smooth point on } B \\ &= 1 \quad \text{for } X_0 \text{ inside } D \end{aligned} \tag{6}$$

To implement the numerical approximation of the Helmholtz integral equation, standard boundary-element procedures are utilized. It is first assumed that the boundary variables can be approximately represented by the interpolation functions,

$$p(\bar{b}) = \Sigma p_j \phi_j(\bar{b}) \tag{7}$$

where p_j is the pressure at a discrete boundary point and $\phi_j(\bar{b})$ a Lagrangian interpolation function. Also,

$$q(\bar{b}) = \Sigma q_j \phi_j(\bar{b}) \tag{8}$$

where q_j is proportional to the normal acoustic velocity at a discrete boundary point. Usually, ϕ_j is only nonzero on a small region of the boundary, i.e., the boundary element. When the interpolations are used in Eq. (1), an approximate boundary integral equation can be written such that

$$cp(\bar{x}_0) = \Sigma p_j \int_B \phi_j(\bar{b}) q^*(\bar{x}_0, \bar{b}) \mathrm{d}B - \Sigma q_j \int_B \phi_j(\bar{b}) p^*(\bar{x}_0, \bar{b}) \mathrm{d}B \tag{9}$$

Equation (9) can be rewritten as

$$cp_0 = \Sigma p_j a_{0j} - \Sigma q_j b_{0j} \tag{10}$$

where

$$a_{0j} = \int_B \phi_j(\bar{b}) q^*(\bar{x}_0, \bar{b}) \mathrm{d}B \tag{11}$$

$$b_{0j} = \int_B \phi_j(\bar{b}) p^*(\bar{x}_0, \bar{b}) \mathrm{d}B \tag{12}$$

To solve a given boundary value problem, $\bar{x}_0$ is moved to each boundary node point in turn. The resulting equations can be rewritten in matrix form as

$$[C]\{p\} = [A]\{p\} - [B]\{q\} \tag{13}$$

where the $[A]$, $[B]$, and $[C]$ are square matrices of dimension N, the number of boundary degrees of freedom, and $[C]$ is a diagonal matrix of the c values for each equation, usually ½. For a well-posed problem, a boundary condition is known at each boundary node. The boundary conditions are applied to Eq. (13), which can be rearranged to yield a fully determined matrix equation of the form

$$[D]\{\alpha\} = \{F\} \tag{14}$$

where the columns of $[D]$ come from either $[A]$ or $[B]$, the elements of $\{\alpha\}$ are the unknown boundary conditions, and the vector $\{F\}$ is computed from the multiplication of columns of $[A]$ or $[B]$ by the known boundary conditions.

When pressures at points on the interior are desired, an equation of the form of Eq. (9) can be written. The boundary solutions p_j and q_j are known from the imposed boundary conditions and the solution of Eq. (14). The position of $\bar{x}_0$ is in the interior of the domain and hence, $c = 1$.

For a straightforward application of the boundary-element methods to the Helmholtz integral equations, either p_j or q_j will be known at each boundary point. However, in most realistic cavity problems (i.e., in aircraft interiors), the boundary pressures are unknown. In addition, boundary acoustic velocities are also not known, particularly on the inside surface of cabin trim treatments where the boundary elements are located. One alternate modeling procedure is to characterize the acoustic behavior of the wall treatments by using specific acoustic impedance. The relationship between

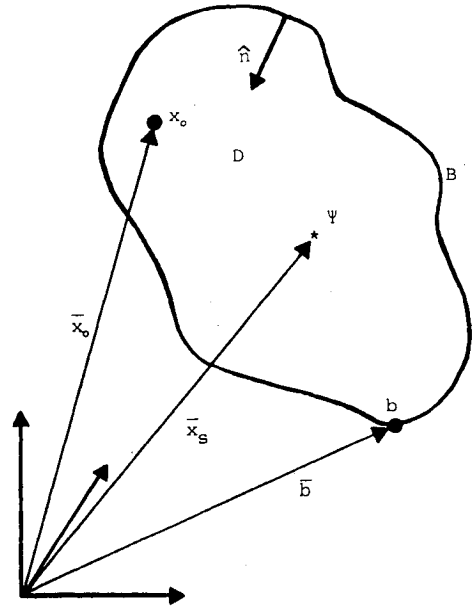

Fig. 1 Geometry of the interior acoustic cavity problem.

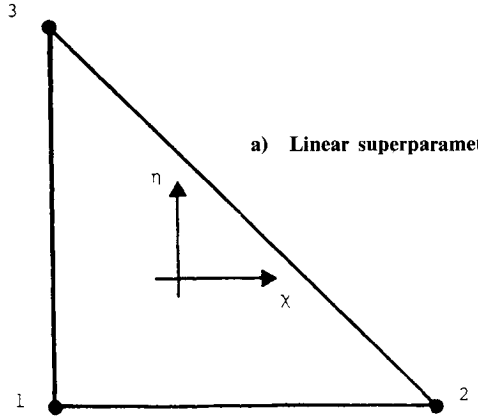

a) Linear superparametric (LS) element.

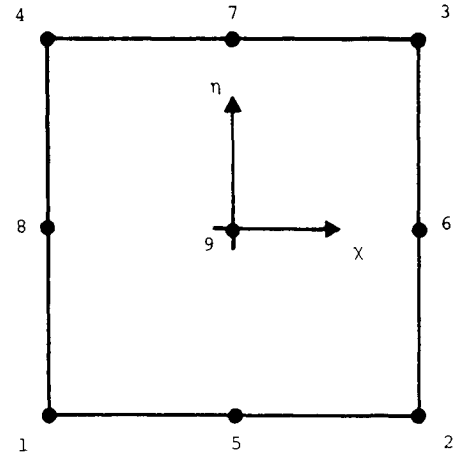

b) Quadratic isoparametric (QI) element.

Fig. 2 Boundary-element parent shapes.

certain discrete boundary pressures in the model and the normal acoustic velocities at the boundary is assumed to satisfy the relationship

$$\{p\} = [Z]\{q\} \tag{15}$$

where the elements of $[Z]$ are related to specific acoustic impedances. The Z matrix is diagonal if locally reacting specific acoustic impedance behavior is assumed. The impedance boundary condition form of Eq. (15) can be incorporated in matrix equation form by replacing the appropriate terms of the p vector in Eq. (13) with the impedance relationship.

Sound sources in the cavity can be incorporated in the model by several techniques. If the source is a reasonably large vibrating surface, it should be modeled as another boundary. The boundary-element method is generalized and the accommodation of such geometry is straightforward. When the source is much smaller than a wavelength, it can be modeled as a point source or monopole. To include point sources in the boundary-element formulation, it is necessary to reconsider the derivation of the Helmholtz integral equation. Equation (1) is derived from the equation

$$\int_D [pL(p^*) - p^*L(p)]\,dD = \int_B (pq^* - p^*q)\,dB \tag{16}$$

where L is a differential operator of the Helmholtz equation,

$$L(p) = \nabla^2 p + k^2 p = 0 \tag{17}$$

In the derivation of Eq. (1), it is assumed the domain is source-free such that

$$L[p(\bar{x})] = 0 \tag{18}$$

and

$$L[p^*(\bar{x}_0,\bar{x})] = \delta(\bar{x} - \bar{x}_0) \tag{19}$$

Thus, the domain integral is

$$\int_D \{p(\bar{x})L[p^*(\bar{x}_0,\bar{x})] - p^*(\bar{x}_0,\bar{x})L[p(\bar{x})]\}\,dD = cp_0 \tag{20}$$

If a point source of strength ψ exists at point $\bar{x}_s$, then

$$L[p(\bar{x})] = \psi\delta(\bar{x} - \bar{x}_s) \tag{21}$$

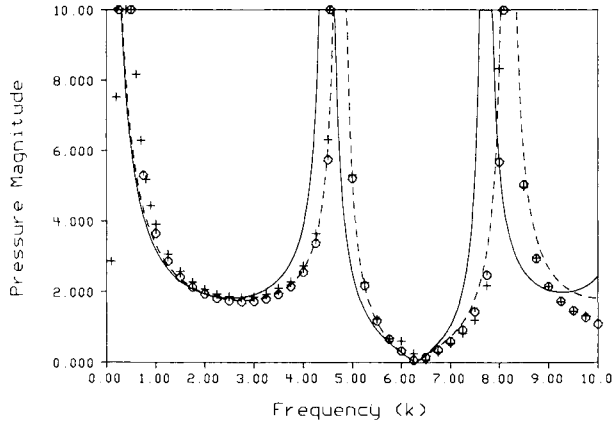

Fig. 3 Pressure at $r = ½$ of a pulsating sphere of radius $a = 1$ with velocity of 1 m/s ($\rho_0 c = 1$): —— analytical solution $a = 1$, - - - - analytical solution ($a = 0.944$), + DBEM solution with 96 LS elements, o IBEM solution with 96 LS elements.

Thus, the domain integral becomes

$$\int_D \{p(\bar{x})L[p^*(\bar{x}_0,\bar{x})] - p^*(\bar{x}_0,\bar{x})L[p(\bar{x})]\}\,dD$$

$$= cp_0 - \psi p^*(\bar{x}_0,\bar{x}_s) \tag{22}$$

In matrix form, Eq. (22) is rewritten as

$$[C]\{p\} - \{Q\} = [A]\{p\} - [B]\{q\} \tag{23}$$

where the terms of Q are

$$Q_j = \psi p^*(\bar{x}_0,\bar{x}_s) \tag{24}$$

The result is a minor change to the solution procedure discussed earlier. The Q vector is added to the F vector of Eq. (14) in order to model the effect of point sources on the cavity sound field.

Indirect Boundary-Element Formulation

The acoustical indirect boundary-element methods (IBEM) are numerical implementations of Huygen's principle. It is assumed that the boundary can be replaced by a fictitious source distribution which will reproduce an identical sound field in the domain. The pressure at any point $\bar{x}_0$ is the integral of the fictitious source distribution multiplied by the fundamental solution for pressure, as

$$p(\bar{x}_0) = \int_B \sigma(\bar{b})p^*(\bar{b},\bar{x}_0)\,dB \tag{25}$$

The fundamental solution is essentially the same as defined in Eq. (3). Acoustic velocity can be found at point $\bar{x}_0$ by the integral of the product of the source distribution and the velocity fundamental solution

$$q(\bar{x}_0) = \int_B \sigma(\bar{b})q^*(\bar{b},\bar{x}_0)\,dB \tag{26}$$

The velocity fundamental solution is essentially the same as that shown in Eq. (5) except that, in general, the velocity in the direction of any vector $\bar{s}$ is found by using

$$q^* = \frac{\partial p^*}{\partial s} \tag{27}$$

Thus, the acoustic velocity anywhere in the domain in any direction can be found. To solve the boundary-value problem, normal velocities at the boundary are used.

For numerical implementation, the source distribution is discretized by the same procedures used earlier for the pressure and velocity variables. The source distribution $\sigma(\bar{b})$ is assumed to be approximately

$$\sigma(\bar{b}) = \Sigma\sigma_j\phi_j(\bar{b}) \tag{28}$$

where σ_j is the value of the source distribution at the jth boundary node. The unknown parameters σ_j are found by applying either Eq. (25) or (26) at a sufficient number of discrete boundary points using known boundary conditions. For example, if p is known at boundary point $\bar{b}_i$, Eq. (25) is used. The boundary integrals are evaluated to develop an equation

$$p(\bar{b}_i) = \Sigma\sigma_j g_{ij} \tag{29}$$

where

$$g_{ij} = \int_B \phi_j(\bar{b}) p^*(\bar{b}, \bar{b}_i) \mathrm{d}B \tag{30}$$

If the normal velocity at point $\bar{b}_i$ is known, then

$$q_n(\bar{b}_i) = \Sigma \sigma_j h_{ij} \tag{31}$$

where

$$h_{ij} = \int_B \phi_j(\bar{b}) q_n^*(\bar{b}, \bar{b}_i) \mathrm{d}B \tag{32}$$

$$q_n^* = \bar{n} \cdot \nabla p^* \tag{33}$$

In matrix form

$$\{p\} = [G]\{\sigma\} \tag{34}$$

$$\{q_n\} = [H]\{\sigma\} \tag{35}$$

If impedance boundary information is known, then

$$\{p\} - [Z]\{q\} = 0 \tag{36}$$

or

$$[[G] - [Z][H]]\{\sigma\} = \{0\} \tag{37}$$

The N unknown discrete values of σ_j are found by applying N boundary conditions using Eqs. (29), (31), or (37). The resulting equations can be written as

$$[D]\{\sigma\} = \{\alpha\} \tag{38}$$

where d_{ij} is either g_{ij}, h_{ij}, or $g_{ij} - Zh_{ij}$, depending on which boundary condition is used and α_i is the value of the boundary condition.

If the pressures or velocities at other points (including boundary points) are desired, the fictitious boundary source distribution can be used in Eq. (29) or (31) to compute the desired solution.

Modeling internal point sources is straightforward for the indirect boundary-element method. A real point source of strength ψ is treated in the same manner as the fictitious sources. The pressure at a point $\bar{x}_0$ is the sum of contributions due to the boundary source distribution and the internal point source.

$$p(\bar{x}_0) = \int_B \sigma(\bar{b}) p^*(\bar{b}, \bar{x}_0) \mathrm{d}B + \psi p^*(\bar{x}_s, \bar{x}_0) \tag{39}$$

where $\bar{x}_s$ is the location of the point source. Similarly, the acoustic velocity is

$$q(\bar{x}_0) = \int_B \sigma(\bar{b}) q^*(\bar{b}, \bar{x}_0) \mathrm{d}B + \psi q^*(\bar{x}_s, \bar{x}_0) \tag{40}$$

Thus, when internal point sources exist, the boundary distribution is found using

$$[D]\{\sigma\} = \{\alpha\} + \{Q\} \tag{41}$$

where Q_i is the appropriate vector term due to internal sources from Eq. (39) or (40).

Boundary Discretization

The boundary-element model of a particular problem is developed by discretizing the boundary of the problem into boundary elements. The boundary integrals of the previous discussion are consecutively evaluated on a piecewise basis over each element. Each element evaluation is performed by mapping the boundary element to a well-defined shape, hereafter called the parent shape. The discretization varies a great deal in complexity, depending on the sophistication of the element. A relatively sophisticated element uses high-order interpolating functions ϕ and is thus capable of closely approximating the physical behavior that varies significantly across an element. Inherent in the mapping procedure is an additional geometric interpolation procedure in which the boundary-element geometry is mapped to the local coordinate system of the parent shape. If the same functions are used for both interpolation procedures, the element is classified as isoparametric. If the mapping interpolation is of higher order than the functional interpolation, the element is classified as superparametric. When the mapping interpolation is of lower order than the functional interpolation, the element is classified as subparametric. In general, more sophisticated elements will be more accurate and require fewer elements to achieve a given level of accuracy. On the other hand, more sophisticated elements require more elaborate evaluation procedures and greater computational time per element. The most efficient element for a given application depends on the complexity of the geometry and the acoustical field.

The two elements used in this investigation will be referred to as the linear superparametric (LS) element whose parent shape is shown in Fig. 2a and the quadratic isoparametric (QI) element whose parent shape is shown in Fig. 2b. For the LS element, the functional interpolation is assumed to be constant over an element, $\phi_j(\bar{b}) = 1$. The mapping interpolation is assumed to be linear such that

$$\bar{b} = \bar{b}(\chi, \eta) \tag{42}$$

The LS element is the simplest three-dimensional boundary element possible and has been used for most of the previous studies of boundary-element acoustics. There is one degree of freedom for each LS element. Thus, the number of degrees of freedom in a model is equal to the number of elements.

The QI element uses quadratic interpolating functions for both the functional and mapping interpolations. The mapping interpolation is quadratic such that $\bar{b} = \bar{b}(\chi, \eta, \chi^2, \chi\eta, \eta^2)$. The interpolation functions in the local coordinate system of the parent shape are

$$\begin{aligned}
\phi_1 &= \tfrac{1}{4}(\chi^2 - \chi)(\eta^2 - \eta) & \phi_6 &= \tfrac{1}{2}(\chi^2 + \chi)(1 - \eta^2) \\
\phi_2 &= \tfrac{1}{4}(\chi^2 + \chi)(\eta^2 - \eta) & \phi_7 &= \tfrac{1}{2}(1 - \chi^2)(\eta^2 + \eta) \\
\phi_3 &= \tfrac{1}{4}(\chi^2 + \chi)(\eta^2 + \eta) & \phi_8 &= \tfrac{1}{2}(\chi^2 - \chi)(1 - \eta^2) \\
\phi_4 &= \tfrac{1}{4}(\chi^2 - \chi)(\eta^2 + \eta) & \phi_9 &= (1 - \chi^2)(1 - \eta^2) \\
\phi_5 &= \tfrac{1}{2}(1 - \chi^2)(\eta^2 - \eta)
\end{aligned} \tag{43}$$

This element has been used in boundary-element investigations by Kipp[13] and Seybert et al.[7] There are nine degrees of freedom for each QI element. In a model constructed of QI elements, however, there is a sharing of grid points between the elements. The number of total degrees of freedom is then equal to the number of grid points in the model, which is somewhat less than nine times the number of elements.

The element discretization can also be used to make the pressure and velocity equal on both elements at the nodes shared by the elements. This effect is referred to as enforcing the compatibility at the interelement boundaries. The finite-element method requires compatibility of the primary variable as part of the formulation of the problem. However, compatibility is not necessarily required for boundary-element methods. In fact, compatibility considerations are

different, depending upon which boundary-element formulation is used. For the DBEM where the functional interpolation is of pressure and velocity, it would seem appropriate that the pressure should be compatible across the element boundaries. On the other hand, the velocity across the element boundaries is discontinuous in many cases. For example, along an edge, the elements on either surface adjacent to the edge will probably have different velocities. A model can be made noncompatible simply by leaving a small gap between the elements. Unfortunately, for standard element discretizations, either compatible or noncompatible elements must be used for both the pressure and velocity interpolation. The QI element used in these investigations is a compatible element. Because the interpolation for the LS element is piecewise constant, the LS element is noncompatible.

In IBEM formulations, the functional interpolation is for the fictitious source distribution. There is no reason for this source distribution to be compatible. Thus, noncompatible elements are acceptable and perhaps even desirable for the IBEM formulations.

An entire family of noncompatible elements exist that can be used for boundary-element studies. These noncompatible elements have nodes only in the interior of the element parent shape. Thus, the functional interpolation is not forced to have the same values on either side of the element boundary. Such elements also avoid the circumstance whereby the boundary conditions are applied at nodes located in extreme locations of the geometry, such as on edges and in corners.

Numerical evaluation of the boundary integrals is also important when considering boundary-element methods. The boundary integrals are evaluated consecutively on a piecewise basis over each element. For most of the elements, standard Gaussian quadrature procedures can be used with reasonable accuracy until the frequency becomes high enough to permit the element characteristic length to approach the wavelength of sound. However, for elements near point x_0 on the boundary, the fundamental solutions contain a singularity and the integrands are not evaluated accurately by Gaussian quadrature. One efficient procedure to evaluate such integrals is to transform the local coordinate system into polar coordinates.[15] In polar form, the radial dependence can be easily integrated analytically. The remaining angular dependence of the integrand is well behaved and can be evaluated accurately using simple Gaussian quadrature procedures.

Results

To verify the adequacy of the boundary-element methods for cavity problems, each element type was tested for several problems with known analytical solutions. The LS element was used for both the IBEM and DBEM formulations. The point source and impedance boundary condition capability were also verified. The QI element was used with the IBEM formulation.

The LS element used to model the interior cavity response is a pulsating sphere with both the DBEM and IBEM formulations. A spherical geometry is one of the most difficult to simulate with the LS element since the boundary is highly curved throughout. The first model used 96 elements. The vertices of the elements were placed on a sphere of one-unit radius. The predicted pressure at one-half the sphere radius is shown in Fig. 3. The solid line is the predicted analytical solution using a sphere radius of one unit. Because the node points are on the sphere, the 96-sided polyhedron resulting from the model is smaller than the sphere. The boundary conditions for this element are actually applied at the centroid of the triangular element. The dashed line shows the analytical solution when the radius of the centroid ($r=0.944$) is used. The computed results are approximately the same as the centroid radius solution. This result is not unexpected, since the boundary-element solutions are much like the collocation solutions; the discretized equations are written to satisfy the boundary conditions applied at a number of discrete points. For the LS elements, the points where the boundary conditions are applied is at the centroid. Thus, the location of the boundary condition points will control the solution accuracy. The predicted solutions for DBEM and IBEM are very similar. In all of the studies made using these elements, no significant difference was found between the IBEM and DBEM solutions.

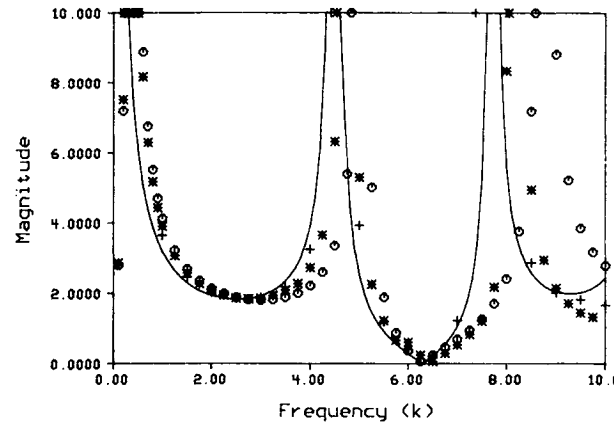

Fig. 4 Pressure at $r=½$ of a pulsating sphere of radius $a=1$ with velocity of 1 m/s ($\rho_0 c=1$): —— analytical solution, o DBEM solution with 48 LS elements, * DBEM solution with 96 LS elements, + DBEM solution with 192 LS elements.

As further evidence that the geometric inaccuracies of the LS model is the source of the frequency shifts illustrated in Fig. 3, additional data were generated using 48, 96, and 192 element models with element vertices on the sphere using the DBEM formulation. The results are shown in Fig. 4. With more elements, the geometry of the sphere is better modeled and the results converge to the analytical solution. However, convergence is slow for the LS element. Unless a different modeling philosophy is used to place the element centroids, it will take many additional elements to lower the error. However, models using a judicious placement of nodes, such that the centroid of the elements are on the surface and the boundary conditions are carefully applied, should be as accurate as the best models of Figs. 3 and 4. For typical aircraft interior geometries with a less sharply curved geometry, it should be relatively easy to develop a good model with the LS element.

In those cases where the geometry of interest is not flat, an element of more sophistication may be more efficient. The pulsating sphere is also modeled using the QI element with an IBEM formulation using 98 nodes and 24 elements. Therefore, this model has 98 degrees of freedom. The QI element does not exactly model the geometry of the sphere, but it is a very close approximation. All of the nodes, where the boundary conditions are to be applied, lie on the sphere surface. The prediction of the acoustic pressure at the surface of the sphere is shown in Fig. 5. The results are much better than any of the LS predictions. The QI element does a much better job of modeling the sphere geometry than the LS element models and produces good results with relatively few degrees of freedom.

In Fig. 5, several points have more significant errors than others. These stray points have been checked and consistently give the same results. No explanation is apparent.

It is also apparent in Figs. 3–5 that the results deteriorate at low frequency for all cases. This result is due to the inadequacy of the integration quadratures used to evaluate the surface integrals. All of the previous results for the LS elements have used a simple one-point integration quadrature. Figure 6 shows the low-frequency results for the LS element

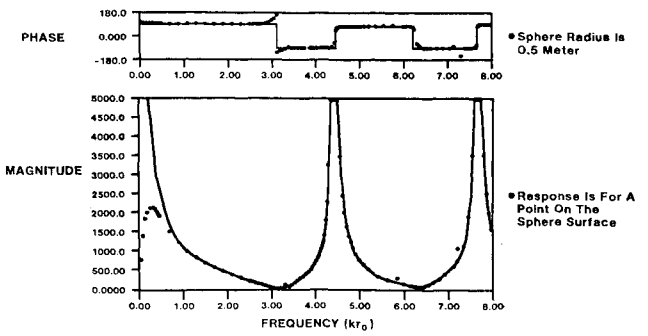

Fig. 5 Pressure at the surface of a pulsating sphere of radius $a = ½$ with velocity of 1 m/s ($\rho_0 c = 415$): —— analytical solution, • IBEM solution with 24 QI elements and 98 degrees of freedom.

with the DBEM program using more sophisticated 4 and 13 point integration quadratures. The results improve significantly. Thus, the low-frequency error can be solved using better integration quadratures at the expense of using more sophisticated integration procedures.

The point source modeling capability was verified by modeling a rigid sphere with a point source at the center. The analytical solution is

$$p(r) = \frac{ik\rho_0 c}{4\pi r} Q\left[\frac{\sin k(r-a) + ka\cos k(r-a)}{ka\cos ka - \sin ka}\right] \tag{44}$$

The results are shown in Fig. 7 for the 48 element LS model and the DBEM formulation. The results follow the analytical solution very well except for the frequency shift illustrated in Figs. 3 and 4 that is caused by the inaccuracy in the geometric models. A low-frequency limit is also apparent, evidently resulting from the integration error since the analysis was done with a one-point quadrature.

The modeling procedures for the impedance boundary condition were verified using a point source in a sphere. In this case, the impedance boundary conditions were used at the sphere surface to simulate the free-field conditions. For spherical radiation, the pressure and velocity are related by

$$p = \frac{ik\rho_0 cr}{1 + ikr} u \tag{45}$$

Thus, the specific acoustic impedance at the surface of a sphere of radius r is

$$z = \frac{ik\rho_0 cr}{1 + ikr} \tag{46}$$

The impedance was applied to the sphere model using the element centroid radius to compute the acoustic impedance. The results using the 48 element LS model and the IBEM formulation are shown in Fig. 8. The results are excellent. The results for this model are better than the earlier ones shown in Figs. 3 and 4 since the element centroids were used to compute the boundary impedances. Similar results were obtained using the DBEM formulation and the QI elements with the IBEM formulation.

To utilize the impedance boundary condition capability of the boundary-element method, the specific acoustic impedance must be known at the model boundary. There are several methods that might be used to determine the specific acoustic impedance of typical cabin trim treatments. The impedance of a small sample can be found using standard impedance tube procedures.[16] However, in many realistic situations, it is not convenient to measure an actual trim sample

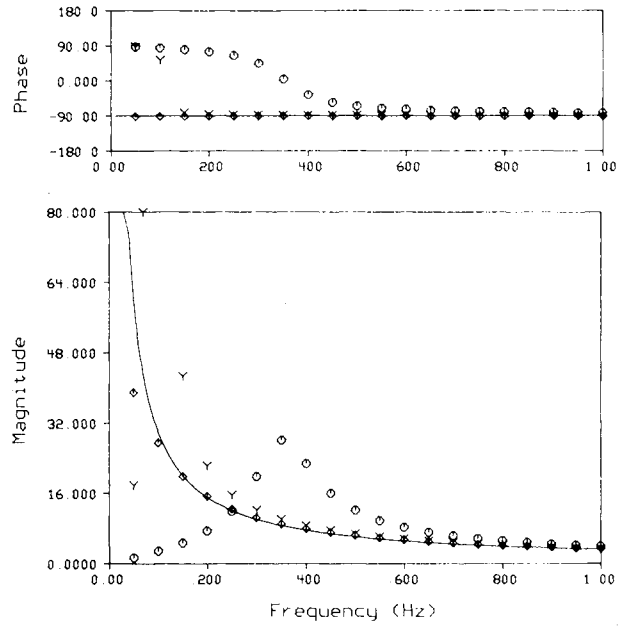

Fig. 6 Pressure at $r = ½$ of a pulsating sphere of radius $a = 1$ with velocity of 1 m/s ($\rho_0 c = 1$) and 96 LS elements (DBEM solution): —— analytical solution, o DBEM solution with 1 point integration quadrature, Y DBEM solution with 4 point integration quadrature, ◇ DBEM solution with 13 point integration quadrature.

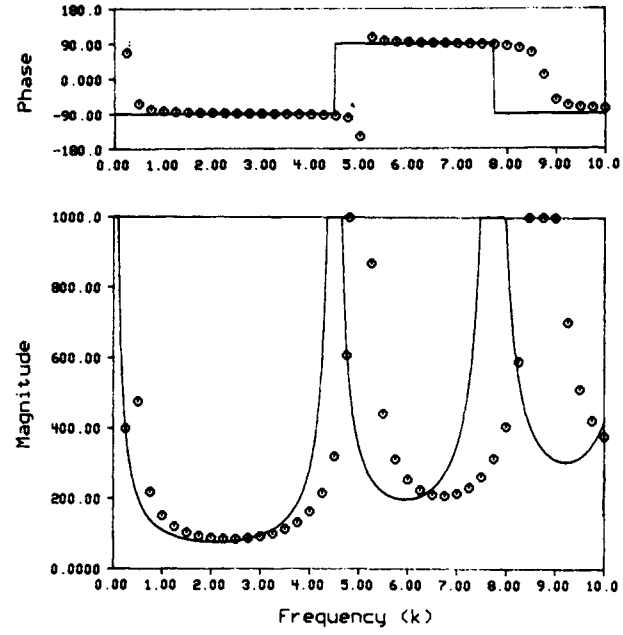

Fig. 7 Pressure at the surface of a rigid sphere of radius $a = 1$ with point source of strength $\psi = 1$ m^3/s at the center of the sphere: —— analytical solution, o DBEM solution with 48 LS elements.

in an impedance tube. Alternatively, two microphone methods can be used, i.e., those described by Chung and Blaser[17] or in ASTM E1050-85a.[18] With extreme care, the two-microphone method may be used "in situ" if necessary. All of these measurement methods assume locally reacting behavior. In many instances, trim treatments are bulk reacting. Significant additional work is necessary to develop either theoretical or experimental procedures that can be used to determine the complete impedance matrix discussed in Eqs. (15) and (36).

One practical aspect of the boundary-element models not addressed here is the discretization requirements of the

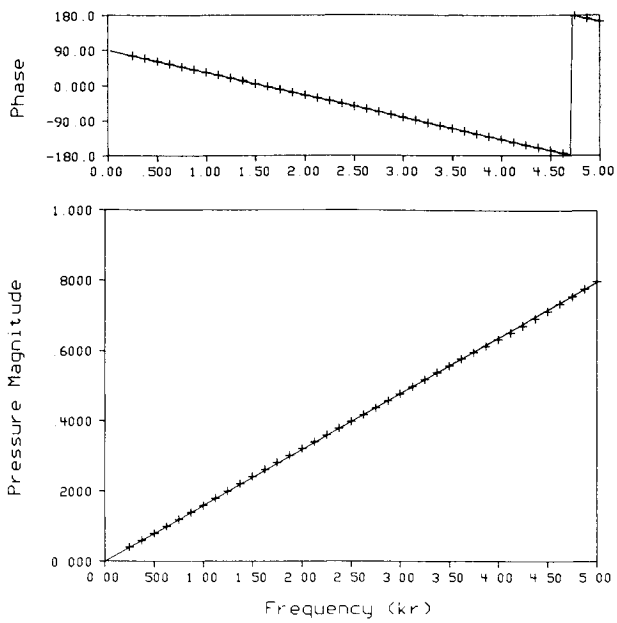

Fig. 8 Pressure at $r = \frac{1}{2}$ of a sphere of radius $a = 1$ with a point source of strength $\psi = 0.5$ m^3/s, and free-field radiation boundary conditions: —— analytical solution, + IBEM solution with 48 LS elements.

methods. As illustrated in this paper, there are high- and low-frequency considerations when using boundary-element methods in cavities. The low-frequency limits can be overcome by using good numerical integration procedures. The high-frequency limits are established by the wavelength of sound and the sophistication of both the integration quadrature and the interpolating functions used. Figures 3 and 5 illustrate the high-frequency limits of the methods. In Fig. 3, the solution begins to diverge from the adjusted analytical solution above $ka = 8$ for a 96 LS element sphere model with a 1 point quadrature. It is difficult to translate this result directly to an element-to-wavelength ratio. However, using a characteristic radius dimension for an individual element, the element characteristic length-to-wavelength ratio at $ka = 8$ is about 0.3. Thus, three or four LS elements per wavelength are required. In Fig. 5, the QI model with 24 elements is still very good at $ka = 8$. The corresponding characteristic length-to-wavelength ratio here is above 0.5. Thus, two QI elements per wavelength should be sufficient. Thus, the boundary discretization can be quite coarse and still produce good results.

Conclusions

The boundary-element formulations of the Helmholtz integral equation and the Huygen's principle have been successfully verified for three-dimensional interior spaces using several spherical geometries. There appears to be little to distinguish the two formulations in the terms of accuracy. The IBEM formulation requires only one boundary integral evaluation in the development of the matrix equation and, thus, the boundary solution is found more economically. However, the boundary solution for the IBEM formulation is a fictitious source distribution. If the boundary solution of acoustic pressure and velocity is desired, numerous postprocessing functions will be necessary and, thus, both methods will have similar computational requirements.

Both a simple [the linear superparametric (LS)] and a sophisticated element [the quadratic isoparametric (QI)] were studied. For the current studies of spherical geometries, the QI models produce better results than the LS models with similar numbers of degrees of freedom. When accuracy is of primary importance and the geometry is not flat, the QI element is better in most circumstances. However, the QI element requires more computations to assemble the model matrices. For flat geometries, the issue of which element is most efficient is not clear.

The formulation of the effects of the interior point sources has been implemented and verified. Such capability is anticipated to be important for the study of active noise control systems in three-dimensional geometries. The formulation of impedance boundary conditions has also been implemented and verified. Impedance boundary conditions can be used to model the effect of cabin trim treatments on the interior sound field. Currently under investigation are numerical procedures that utilize the impedance boundary condition capability of the DBEM to identify the acoustic behavior in a cavity under operating conditions and, consequently, to identify the noise sources in the cavity.

Acknowledgment

This work was supported by NASA Grant NAG1-58.

References

[1]Unruh, J. F., "Finite Element Subvolume Technique for Structure Borne Interior Noise Prediction," *Journal of Aircraft*, Vol. 17, 1979, pp. 434–444.

[2]Nefske, D. J., Wolf, J. A. Jr., and Howell, L. J., "Structural-Acoustic Finite Element Analysis of the Automobile Passenger Compartment—A Review of Current Practice," *Journal of Sound and Vibration*, Vol. 80, No. 2, 1982, pp. 247–266.

[3]Chen, L. H. and Schweikert, D. G., "Sound Radiation from an Arbitrary Body," *Journal of the Acoustical Society of America*, Vol. 35, No. 10, 1963, pp. 1626–1632.

[4]Chertock, G., "Sound Radiation from Vibrating Surfaces," *Journal of Acoustical Society of America*, Vol. 36, No. 7, 1964, pp. 1305–1313.

[5]Copley, L. G., "Fundamental Results Concerning Integral Representations in Acoustic Radiation," *Journal of Acoustical Society of America*, Vol. 44, No. 1, 1968, pp. 28–32.

[6]Schenck, H. A., "Improved Integral Formulation for Acoustic Radiation Problems," *Journal of Acoustical Society of America*, Vol. 44, No. 1, 1968, pp. 41–58.

[7]Seybert, A. F., Soenarko, B., Rizzo, F. J., and Shippy, D. J., "Application of the BIE Method to Sound Radiation Problems Using an Isoparametric Element," *ASME Transactions, Journal of Vibrations, Acoustics, Stress, and Reliability in Design*, Vol. 106, 1984, pp. 414–420.

[8]Burton, A. J. and Miller, G. F., "The Application of Integral Equation Methods to the Numerical Solution of Some Exterior Boundary Valve Problems," *Proceedings of the Royal Society of London*, Vol. A323, 1971, pp. 201–210.

[9]Koopmann, G. H. and Benner, H., "Method of Computing the Sound Power of Machines Based on the Helmholtz Integral," *Journal of Acoustical Society of America*, Vol. 71, No. 1, 1982, pp. 78–89.

[10]Astley, R. J., "Acoustic Radiation in Low Mach Number Flows: A Transformed Boundary Element Approach," AIAA Paper 84-2288, 1984.

[11]Tanake, T., Fujikawa, T., Abe, T., and Utsuno, H., "A Method for the Analytical Prediction of Insertion Loss of a Two-Dimensional Muffler Model Based on the Transfer Matrix Derived from the Boundary Element Method," ASME Paper 84-WA/NCA-7, 1984.

[12]Banerjee, P. K. and Butterfield, R., *Boundary Element Methods in Engineering Science*, McGraw-Hill, London, 1981.

[13]Kipp, C. R., "Prediction of Sound Fields in Acoustical Cavities Using the Boundary Element Method," M.S. Thesis, Purdue University, West Lafayette, IN, 1985.

[14]Kipp, C. R. and Bernhard, R. J., "Prediction of Acoustical Behavior in Cavities Using an Indirect Boundary Element Method," *ASME Transactions, Journal of Vibrations, Acoustics, Stress, and Reliability in Design*, Vol. 109, 1987, pp. 22–28.

[15]Zimmerle, D. J. and Bernhard, R. J., "Integration of Certain Singular Boundary Element Integrals for Applications in Linear Acoustics," Purdue University, West Lafayette, IN, Herrick Laboratory Rept. HL 85-12, 1985.

[16]"Standard Test Method for Impedance and Absorption of Acoustical Materials by the Tube Method," American Society for Testing and Materials, Philadelphia, ASTM C384-77, 1977.

[17]Chung, J. Y. and Blaser, D. A., "Transfer Function Method for Measuring In-Duct Acoustic Properties: I. Therory and II. Experiment," *Journal of Acoustical Society of America*, Vol. 68, No. 3, 1980, pp. 907-921.

[18]"Standard Test Method for Impedance and Absorption of Acoustical Materials Using a Tube, Two Microphones, and a Digital Frequency Analysis System," American Society for Testing and Materials, Philadelphia, ASTM E1050-85a, 1985.

From the AIAA Progress in Astronautics and Aeronautics Series...

FUNDAMENTALS OF SOLID-PROPELLANT COMBUSTION – v. 90

Edited by Kenneth K. Kuo, The Pennsylvania State University
and
Martin Summerfield, Princeton Combustion Research Laboratories, Inc.

In this volume distinguished researchers treat the diverse technical disciplines of solid-propellant combustion in fifteen chapters. Each chapter presents a survey of previous work, detailed theoretical formulations and experimental methods, and experimental and theoretical results, and then interprets technological gaps and research directions. The chapters cover rocket propellants and combustion characteristics; chemistry ignition and combustion of ammonium perchlorate-based propellants; thermal behavior of RDX and HMX; chemistry of nitrate ester and nitramine propellants; solid-propellant ignition theories and experiments; flame spreading and overall ignition transient; steady-state burning of homogeneous propellants and steady-state burning of composite propellants under zero cross-flow situations; experimental observations of combustion instability; theoretical analysis of combustion instability and smokeless propellants.

For years to come, this authoritative and compendious work will be an indispensable tool for combustion scientists, chemists, and chemical engineers concerned with modern propellants, as well as for applied physicists. Its thorough coverage provides necessary background for advanced students.

Published in 1984, 891 pp., 6×9 illus. (some color plates), $60 Mem., $85 List; ISBN 0-915928-84-1

TO ORDER WRITE: Publications Order Dept., AIAA, 370 L'Enfant Promenade, SW, Washington, DC 20024